Improved wear behaviour of alumina-aluminium titanate laminates with low residual stresses and large grained interfaces

S. Bueno[1,2,3,*], L. Micele[2], C. Melandri[2], C. Baudin[1], G. De Portu[2]

[1] Instituto de Cerámica y Vidrio, CSIC. Kelsen 5. 28049. Madrid. Spain

[2] Istituto di Scienza e Tecnologia dei Materiali Ceramici, CNR. Via Granarolo 64. 48018. Faenza (RA). Italy

[3] Fundación Innovarcilla – Centro Tecnológico de la Cerámica de Andalucía. Pol. Ind. El Cruce, Los Alamillos, 25. 23710. Bailén (Jaén). Spain

Abstract. The wear behaviour of a monolithc alumina and an alumina-aluminium titanate laminated structure was studied. The laminate, containing surface fine grained alumina layers and internal composite layers with 10vol.% of aluminium titanate, showed relatively low (≅20 MPa) compressive residual stresses at the surface. Interfaces between layers were constituted by large alumina grains (up to ≅50 μm) that promoted toughening due to crack deflection and branching. Wear tests were performed on square specimens (30 x 30 x 6 mm^3) using the pin-on-disc method. The laminates showed higher wear resistance than the monolithic alumina. The analysis of the results together with SEM-EDX observations was performed to identify possible wear mechanisms. The wear resistance improvements are discussed in terms of the residual stresses in the laminate and the properties provided by the special microstructure of the interfaces.

Keywords: *Microstructure; Wear resistance; Al_2O_3; Al_2TiO_5; Laminates*

* Corresponding author.
E-mail address: materiasprimas@innovarcilla.es (S. Bueno)

1. Introduction

Ceramic materials can significantly improve the response of components and pieces for applications involving contact loadings due to their high hardness, potentially low friction, excellent corrosion resistance and ability to operate under extreme conditions as high temperatures. In particular, alumina materials are widely considered to be excellent candidates for wear-resistant components due to their high hardness.[1] However, the potential of alumina in many applications is limited by its inherent brittleness and, thus, the risk of catastrophic failure at highly variable loads.[1,2]

As an alternative to monolithic materials, the laminated configuration arise as a microstructural design strategy, that may be defined as extrinsic, for developing more flaw tolerant ceramic materials. In laminates, a suitable combination of layers with different compositions or microstructures yield improved mechanical response with respect to that exhibited by each individual layer.[3,4] The design approaches proposed for laminates with elevated mechanical performance may be classified in three large groups[3,4], each of them resulting in materials with different characteristics.

In a first group, it has been shown that laminated structures can be properly designed on the basis of the development of surface compressive residual stresses during cooling from the sintering temperature, giving rise to large improvements in strength and surface toughness[5,7] but associated with a limited flaw tolerant behaviour. Strength increases play an important role in improving the wear resistance of ceramics[1,8] and, in particular, the effectiveness under wear of laminated ceramics of alumina/zirconia with compressive surface stresses has already been discussed in relation to the corresponding stress-free material.[9] These materials are suitable for structural applications within the temperature range where the above mentioned residual stresses are significant.

On the other hand, on the basis of the toughening mechanisms identified for stress free natural structures, residual stress free laminated materials with stiff layers separated by weak interfaces combine both high strength and a pronounced flaw tolerant behaviour because the potential activation of crack deflexion along the interfaces before penetrating the contiguous layer.[10,11] Although these materials are good candidates for some structural and thermal applications, they are not adequate for wear applications because these imply shear stresses that lead to delamination, which is then favoured by the presence of weak interfaces.[10]

A third group of residual stress free laminated materials with strong interfaces between high strength, stiff and hard surface layers and weak, heterogeneous and/or microcracked (i.e. flaw tolerant) internal ones combine the better of the two approaches just described. These materials would be ideal for applications involving contact and thermal loadings, because they could develop internal zones of diffuse damage, avoiding an effective surface structural degradation of the material.[12-14] The basic requirements for this family of laminates are that the microstructures of the layers have to provide fundamentally different modes of crack control while the possibility of tensile residual stresses in the external layers is minimised.[3]

According to this last design approach, an alumina-aluminum titanate laminated structure with relatively low compressive surface residual stresses[15] was developed in a previous work.[14] This structure showed homogeneous and fine grained surface alumina layers and heterogeneous and relatively weak internal interfaces (Fig. 1). The fracture toughness was similar to that of monolithic alumina materials obtained using the same conditions (Table 1) while the work of fracture (Table 1) was significantly higher than that obtained by calculation, taking into account the additive character of the work of fracture, from the work of fracture values of monolithic materials of the same composition of the layers. This fact revealed a synergic effect of the laminated structure on the mechanical behaviour of the material. The most important difference between this laminated structure, and other laminates

with high capability for crack deflection, was that the crack deflection and branching processes occurred at local level. As a consequence, relatively high apparent toughness and work of fracture could be obtained while maintaining the structural integrity of the piece after the initiation of crack propagation under shear stresses as those that develop in wear applications. These mechanical properties allowed inferring the suitability for contact loading applications. In this work, wear tests were performed on such laminated structure and on a reference monolithic alumina material. Results are discussed in terms of the residual stresses and the properties supplied by the special microstructure of the interfaces.

2. Experimental

A monolithic material of monophase alumina and one layered structure combining two external and one central alumina layers with two internal alumina+10vol.% aluminium titanate composite layers (Fig. 1) were manufactured by colloidal filtration from aqueous alumina, Al_2O_3, and titania, TiO_2, suspensions using the optimum green processing conditions established elsewhere.[16] The starting materials were commercial α-Al_2O_3 (Condea, HPA05, USA) and TiO_2-anatase (Merck, 808, Germany) powders. The powders were dispersed in deionised water by adding 0.5 wt.% (on a dry solids basis) of a carbonic acid based polyelectrolyte (Dolapix CE64, Zschimmer-Schwarz, Germany). Suspensions were prepared to a solids loading of 50 vol.% and ball milled with alumina jar and balls during 4h.

Monolithic and layered plates (≈70x70x10 mm^3) were obtained by slip casting, removed from the moulds and dried in air at room temperature for at least 24h. The layered plates, constituted by five layers (Fig. 1) were fabricated by alternately casting the suspensions.[16] Sintering of the plates, in air in an electrical box furnace (Termiber, Spain), was performed at 1550ºC-3h at heating and cooling rates of 2ºCmin^{-1} and with 4h dwell at 1200ºC during heating.

Densities of the sintered compacts were determined by the Archimedes's method in water (European Standard EN 1389:2003) and the relative density for monolithic alumina materials was calculated considering 3.99 $g \cdot cm^{-3}$ as theoretical density (ASTM 42-1468). The densities of the different layers in the laminate were also determined by the Archimedes's method in water after sequential removing of the layers by grinding. Density values were calculated from the difference between that of the complete laminate specimen and those of the specimen once each layer was removed, relative densities could be calculated taking into account the fraction of layer thickness. The theoretical density of alumina+10vol.% aluminium titanate composite layers was calculated from the alumina and the aluminium titanate (3.70 $g \cdot cm^{-3}$, ASTM 26-0040) theoretical densities. Reported densitiy values are the average of five measurements and errors are the standard deviations.

The true average grain size was determined by the linear intercept method on microstructural images performed by field emission gun scanning electron microscopy (FEG-SEM, Hitachi, S-4700, Japan) on polished and thermally etched surfaces, considering at least 200 grains for each phase and using the correction factor $4/\pi$.

Vickers indentation tests were performed on polished surfaces at 50 N (Microtest, Spain) holding the load for 10 s. Optical microscopy (Carl-Zeiss H-P1, Germany) was performed on the indented samples and hardness (H_V) was calculated from the applied load and the projected areas of the residual impressions determined from the length of the diagonal according to equation: $H_V = 2 \cdot P/(2 \cdot d)^2$, where P is the applied load and $2 \cdot d$ is the length of the diagonal.

Young's modulus of the alumina material was determined from the resonance frequency of bars tested in flexure (Grindosonic model MK 5, J.W. Lemmens, Leuven, Belgium); the sample size was 4x6x50 mm^3. The same determinations were done on laminated specimens to determine the apparent Young´s modulus of the laminate.

Fracture toughness and work of fracture were determined by 3 point bending tests on Single Edge V Notch Beams (SEVNB) of 4x6x50 mm^3 as described previously.[14]

Reported grain size, hardness, Young`s modulus, fracture toughness and work of fracture values are the average of at least three measurements and errors are the standard deviations.

Sliding wear tests were conducted on square samples (30 x 30 x 6 mm^3) using an inverted pin-on-disk configuration on a tribometer (Wazau, Berlin, Germany) in unlubricated conditions (Fig. 2). Commercial hemispherically-tipped pins of 7 wt.% cobalt-bonded tungsten carbide (WC) (ISO K20) were employed (diameter: 5 mm, density: 14.85 g/cm^3, hardness: 20.0 GPa) with a surface roughness R_a = 0.13. The sample rotated above the fixed pin and the load was applied by a lever arm. The ceramic plates (≈70x70x10 mm^3) were machined to get parallel surfaces. The surface roughness of such ground surfaces, measured by a profilometer (Taylor Hobson, Talysurf Plus, UK) was R_a = 0.19 ± 0.03 μm. The applied load was 50 N and the sliding speed 0.5 m/s. The total sliding distance was 10 km for all the tests with a wear track diameter of 20 mm. The torque and the applied load were continuously recorded during the test with a computer data acquisition program. The temperature and humidity of the laboratory atmosphere were kept in the range of 22 ± 1 ºC and 50 ± 10%, respectively. Before testing, the samples and pins were cleaned in an ultrasonic bath with acetone for 15 min and then dried at 100°C for 30 min. After 1 h of natural cooling, the samples and pins were weighed using a balance with an accuracy of 10^{-5} g. After testing, the samples were cleaned using the same procedure described above and weighed again. The specific wear of the specimens was evaluated using two techniques: from the mass loss normalized dividing by the applied load and the sliding distance, and from the volume loss. For this one, the depth of the wear tracks was measured in four positions, 90° apart, perpendicularly to the wear track, by profilometer (Taylor Hobson, Talysurf Plus, UK). The depths of the tracks were integrated using the profilometer software to obtain the wear scar

area, then averaged and multiplied for the track length. The dislodged volume was then normalised by the applied load and the sliding distance. The specific wear of the pin was evaluated using the same methods: the mass loss technique and the volumetric one. In this last case the volumes lost by the pins were calculated from their dimensions and the diameter of the worn surface. At least three tests were performed for each material. The torque value was continuously monitored during the tests but the first part (running-in), was not considered for the friction coefficient calculation.

The features of the wear track were analysed using a scanning electron microscope (SEM, Cambridge Instruments, Stereoscan 360, UK) coupled with analysis by dispersive energies of X-ray (EDX, Oxford Instruments, Inca Energy 300, UK).

3. Results

3.1 Microstructure and materials properties

The laminated structure containing surface alumina layers is schematically represented in Fig. 1. The compressive residual stresses at the surfaces were determined to be about 20 MPa.[15]

Characteristic microstructures of the materials are shown in Fig. 3 and the microstructural parameters are summarised in Table 1. The alumina monolithic materials (Fig. 3a) presented bimodal microstructure with some grains larger than 10 μm and the rest of the grains in the range described by the average size determined by the linear intercept method (Table I).

The main features of the microstructure of the laminated structure are shown in Fig. 3b,c. The thickness of the large grain sized alumina interfaces was about 150 μm (Fig. 3b). These interfaces had extremely bimodal microstructures, constituted of groups of small (≅2-3μm) grains surrounded by very large (>20-30 μm, Fig. 3c) ones. The external and central fine

grained alumina layers presented microstructures similar to those of the monolith (Fig. 3a, Table I).[14]

In Table I, the values of hardness, fracture strength, fracture toughness and work of fracture are collected. The laminate showed slightly larger fracture toughness values than the reference alumina material due to the surface compressive residual stresses. Also, the external alumina layer of the laminate presented higher hardness values with lower dispersion. The increased the work of fracture as compared to that of the reference alumina was due to the toughening mechanisms (limited crack deflection and branching) associated to the large grained alumina interface, as described previously.[14]

3.2 Wear tests

The average stationary values of the coefficient of friction, μ, achieved after a running-in period of variable duration (≈1 hour) and measured for the different sliding pairs, were 0.58 ± 0.04 and 0.51 ± 0.04 for the monolithic alumina and the laminate, respectively.

Table II reports the specific wear rates in a weight and volumetric base for both discs and pins. The pins slid against the laminates showed the lowest wear rate. Following the same trend, the wear of the laminated specimens is also lower than the values measured on the monolith. Volumetric average values of $(1.2 \pm 0.4)\cdot 10^{-7}$ and $(7.0 \pm 0.2)\cdot 10^{-8}$ $mm^3/m\cdot N$ were determined for monolith and laminate, respectively (Table II). As the results based on the weight method showed a very high scatter, the results obtained by volumetric method were taken in to account.

Characteristic worn surfaces of the pins and the ceramic specimens are showed in Fig. 4 and Fig. 5, respectively. Pins slid against the monolithic alumina (Fig. 4a,b) showed a grooved pattern (Fig 4a) and compacted particles along the half edge of the worn surface in the sliding direction (dark grey particles in Fig. 4b). On the contrary, worn surfaces of pins

slid against the laminate (Fig. 4c) presented a significantly smaller number of grooves and mostly “clean” edges without compacted particles.

The wear tracks of the monolithic specimens (Fig. 5a) were wider than those of the laminates (Fig. 5b). In both materials, the track was almost covered by a compacted layer interrupted by the presence of zones of the underlying surface showing mostly intergranular fracture (Fig. 5c,d). The monolithic alumina specimens (Fig. 5a) showed a central strip in a lighter grey shade in which fractures smeared in the sliding direction were more extensively showed.

4. Discussion

The average wear rate values determined for the monolithic alumina material ($2.3 \cdot 10^{-9}$ g/m·N and $1.2 \cdot 10^{-7}$ mm^3/m·N, Table II) agree with those reported for alumina materials with similar grain size under various wear configurations[17-19] taking into account that wear is a test system-configuration property and that large data dispersion has been reported in pin on disk tests performed inter and within laboratories.[1,20]

The examination of the wear tracks in Fig. 4 and 5, gives an indication of the wear mechanisms that occurred. The compacted particles along the half edge of the worn surface in the sliding direction (dark grey particles in Fig. 4b) of pins slid against the monolithic alumina showed high Al contents, indicating a mass transfer from the ceramic disc to the pin. The layers adhered to the surface of the tracks in the ceramic discs (Fig. 5) are the result of the compaction of debris particles from the pin and the ceramic specimen, as demonstrated by the fact that the semiquantitative microprobe analysis (EDX) performed on the wear track of the samples showed some material transfer from the WC pin to the ceramic disc (Fig. 5e). The mostly intergranular fractures observed in the underlying surface (Fig. 5d) suggest the wear process to proceed by grain boundary microcracking, grain dislodgement, comminution of the

removed grains between the sliding surfaces, plastic deformation of the debris giving rise to the adhered layer along the wear track and, finally, partial delamination of this layer. This wear mechanism was found to be the same for both the alumina monolith and the laminated material and has been observed in similar ceramic wear tests.[17,21-23]

In spite of the similar wear mechanism for both materials, the pins slid against the laminates showed lower average wear rates (Table II). This trend was also observed for the discs ($f = W_{LAM}/W_A \approx 0.6$, Table II). However, the experimental scatter does not allow reaching definite quantitative conclusions about differences between the laminated and monolithic specimens. Therefore, a deeper analysis of both materials must be performed. The debris compacted layer along the wear track (Fig. 5a,b) showed mainly two grey shades that were randomly distributed (Fig. 5b) in the laminated specimens whereas a larger area of the lighter shade, preferentially oriented along a central strip, was observed in the monolithic alumina (Fig. 5a). The qualitative EDX analysis performed on both shades (Fig. 6) revealed significantly larger WC contents in the lighter shade and, thus, a larger material transfer from the WC pin to the ceramic monolith. The increased amount of debris formed during sliding of the monolithic-pin pair offers a large contact surface for both materials (pin and ceramic), thus leading to an increase in adhesive friction ($\mu = 0.58$ and 0.51 for monoliths and laminates, respectively) as reported elsewhere.[21] These SEM observations of the worn tracks, revealing the different wear damage extension in laminated and monolithic specimens agree with the higher average wear rate of the monolithic specimens qualitatively deduced from data in Table II). Therefore, even though the average experimental values presented relatively high scatter, the discussion of the causes of such qualitative differences on the basis of the average experimental values has been considered to be valid.

First, the differences of the mechanical properties between monolith and laminate (Table I) is considered as a possible reason for the better behaviour of the last. In order to discern

whether such improvement was only caused by the better mechanical properties of the laminated structure, the overall effect of the mechanical properties on the wear resistance can be evaluated by Evan`s method[23,24], by which a quantitative evaluation of the increase of wear can be made in terms of the mechanical properties such as toughness, hardness and Young's modulus (Eq. 1):

$$V = a \cdot \frac{F^{9/8}}{K_{IC}^{1/2} \cdot H^{5/8}} \cdot \left(\frac{E}{H}\right)^{4/5} \cdot L \qquad (1)$$

where V is the wear volume, F the applied load, K_{IC} is the fracture toughness, H the hardness, a the constant which is independent of the material type, E the Young's modulus, and L is the sliding distance. The expected ratio of the wear rate of the laminate to that of the alumina monolith can be obtained by employing Eq. 1 and the result is shown in Table II ($f_{calc} \approx 0.9$). This value is higher than the one calculated from the average experimental values and, thus, it does not reflect the decrease of the experimental wear rate of the laminate. Therefore, when average experimental values are considered, the improved mechanical properties of the laminated material could just explain a part of the improvement of the wear resistance, mainly due to the improved fracture toughness as there were negligible differences in the hardness and Young's modulus of the monolithic and laminated samples (Table I).

Effectively, as described elsewhere[9], because the wear process is dominated by brittle fracture, the fracture toughness is considered to be a primary parameter to relate to the wear loss. For a material with a given flaw size, the critical condition for the onset of cracking at the surface occurs when the stress intensity factor due to the maximum principal tensile stress, is greater or equal to the local fracture toughness. The presence of compressive residual stresses increases the apparent surface fracture toughness and, since it opposes the tensile stress generated in the wake of the sliding contact, it prevents the formation and propagation

of cracks. As a result, there were more fractured grains available for erosive wear in the pin – monolithic alumina couple, thus explaining the grooved pattern in the pin and the higher WC contents inside the wear track of monolithic samples (Fig. 4a,b). As described in the work by De Portu et al.[25], dense alumina samples tested in abrasive wear regime clearly show how an increase in the surface residual compressive stresses leads to a lower wear volume.

Another possible explanation for the different wear resistance of monolith and laminate is the thermal effect that takes place in the couplings during the tests. In the disk wear track, the heat dissipation at the contact point is determined by the thermal conductivity (Fig. 7). In Fig. 8 relative density values for the layers in the laminated structure, determined by sequentially removing the layers by polishing, are represented. These values are compared to that of the reference alumina material. Both monolith and surface layers present relative density values about 98% of alumina theoretical density. Internal composite alumina-aluminium titanate layers in the laminated structure present a relative density of about 97-98% of theoretical (Fig. 8). Such dense microcrack free alumina-aluminium titanate composite would show thermal conductivity and diffusivity values similar to that of alumina, as determined elsewhere.[26] However, next to the external alumina layer there is a large grained alumina interface whose relative density values (Fig. 8) indicate a void volume, porosity and/or microcracks, of about 9 %. Such relatively porous alumina would present a value of thermal conductivity up to 20% lower than that of dense alumina materials.[27] It is hypothesised that, due to this increased insulating behaviour, the contact temperature in the laminated disk could be higher than that in the monolithic sample.[22]

A rough calculation of possible additional heating of the worn surface in the laminate due to the refractory behaviour of porous interfaces can be estimated from the heat flux schematically represented in Fig. 7. The heat dissipation (Q) along the bulk monolithic specimen is quantified by Eq. 2:

$$Q = K \cdot t \cdot (T - T_r) \quad (2)$$

where K is the thermal conductivity of the monolithic dense alumina specimen, t is the specimen thickness, T is the temperature in the worn surface and T_r is room temperature. In the case of the laminated specimen (Eq. 3 and 4) [28]:

$$Q = K' \cdot t \cdot (T' - T_r) \quad (3)$$

$$\frac{1}{K'} = \frac{t_{A+AT}}{K} + \frac{t_I}{0.8 \cdot K} \quad (4)$$

where K' is the thermal conductivity of the laminated specimen, t_{A+AT} and t_I represent the volumetric fraction of dense alumina-aluminium titanate layers and porous interfaces, respectively, and K is the thermal conductivity of dense alumina and aluminium titanate layers. The thermal conductivity of porous interfaces is considered to be approximately 80 % of thermal conductivity of dense alumina. Taking into account the laminated geometry (t_{A+AT} is 0.86 and t_I is 0.14), Eq. 4 leads to $K' = 0.97 \cdot K$.

For a calculation purpose, a flash temperature of approximately 500 ºC, as described elsewhere[21,29], has been considered to be easily achieved during wear processes on ceramic specimens. According to Eq. 2, the heat dissipation (Q) generated along a monolithic dense alumina (K=15 W/(m·K) [27]) sample (t=6mm) would be $Q \approx 43$ W, assuming an average value of K independent from the temperature gradient along the specimen.

A heat flux similar to that calculated for the monolithic specimen ($Q \approx 43$ W) transmitted along the laminated sample, with a lower thermal conductivity ($K' \approx 0.97 \cdot K$), would lead,

according to Eq. (3), to a value of T' of approximately 517ºC. So, the increase of temperature expected from the insulating behaviour of the interfaces in the laminated specimen would be negligible and would not influence the different wear rate showed by the monolithic and the laminated specimens.

To summarize, from the different possibilities studied to explain such different wear resistances, in spite of the similar wear mechanisms, the higher fracture toughness associated to surface compressive residual stress developed in the laminate appears to be, at least in part, responsible of the improved behaviour in the laminated specimen. However, as discussed previously on the basis of average experimental values, this improvement is larger than expected from the bettered mechanical properties in the laminate. Concerning this discussion, it also has to be emphasized that even though hardness values of the monolithic and the laminate are statistically the same, hardness of the monolithic alumina is highly variable, that must be related to other parameters: the higher fracture toughness of the laminate (Table I) and/or different surface microstructure. In fact, there are some large grains (≈10 μm) in the monolithic (Fig. 3a) whereas the microstructure of the alumina layer is homogeneous in the laminate.

This slight microstructural difference observed in the laminate (more homogeneous microstructure in the surface alumina layer) would also explain the improved wear resistance. The model of Evans[30] for wear (system of indenters) considers the continuum, thus, there is no effect of the grain size in the formation of the indentation lateral cracks that would run to the surface and originate material loss. In real materials with intergranular fracture such as alumina, the lateral cracks originate at the grain boundaries and thus, the volume of material loss increases with grain size. As a matter of fact, generally large grained materials have lower wear resistance. In fact when the wear mechanism is due to microcracking at grain boundaries with consequent grain removal, larger is the grain higher is the removed volume.

5. Conclusions

The results of some preliminary experiments exploring the wear resistance of an alumina-aluminium titanate flaw tolerant laminated structure with low residual stresses are presented.

The wear mechanism of the laminate is the same as that of a reference monolithic alumina fabricated using the same conditions as that of the laminate and, thus, with similar microstructural parameters.

The laminate presents higher wear resistance in terms of total volume loss of material, the possible factors responsible for this behaviour are:

1) The higher fracture toughness in the laminate associated to surface compressive residual stress developed in the surface layers.
2) The more homogeneous microstructure of the surface alumina layers in the laminate as compared to that of the alumina monolithic material with some grains larger than 10 μm and the rest of the grains in the range of those showed by the alumina layers in the laminate.

Acknowledgments

The financial support of the Project MEC MAT2006-13480 C02 and the Postdoctoral Fellowship MEC EX-2006-0555 (Spain) is acknowledged.

References

1. Rainforth WM. The wear behaviour of oxide ceramics-A Review. J Mater Sci 2004; **39**: 6705-6721.

2. Hutchings IM. TRIBOLOGY: Friction and Wear of Engineering Materials. London: Hodder Headline PLC; 1992.

3. Bueno S, Baudín C. Flaw Tolerant Ceramic Laminates with Negligible Residual Stresses between Layers. Key Engineering Materials 2007; **333**: 17-26.

4. Chan HM. Layered Ceramics: Processing and Mechanical Behavior. Annu Rev Mater Sci 1997; **27**: 249-82.

5. Virkar AV, Huang JL, Cutler RA. Strengthening of Oxide Ceramics by Transformation-Induced Stresses. J. Am Ceram Soc 1987; **70**: 164-170.

6. De Portu G, Micele L, Guicciardi S, Fujimura S, Pezzotti G, Sekiguchi Y. Effect of residual stresses on the fracture behaviour of notched laminated composites loaded in flexural geometry. Composites Science and Technology 2005; **65:** 1501-1506.

7. Gurauskis J, Sánchez-Herencia AJ, Baudín C. Alumina-zirconia layered ceramics fabricated by stacking water processed green ceramic tapes. J Eur Ceram Soc 2007; **27:** 1389-1394.

8. Adachi K, Kato K, Chen N. Wear map of ceramics. Wear 1997; **203-204**: 291-301.

9. Toschi F, Melandri C, Pinasco P, Roncari E, Guicciardi S, De Portu G. Influence of Residual Stresses on the Wear Behaviour of Alumina/Alumina-Zirconia Laminated Composites. J Am Ceram Soc 2003; **86**: 1547-53.

10. Clegg WJ. Controlling Cracks in Ceramics. Science 1999; **286:** 1097-1099.

11. Kuo DH, Kriven WM. Fracture of multilayer oxide composites. Materials Science and Engineering 1998; **A241:** 241-250.

12. Russo CJ, Harmer MP, Chan HM, Miller GA. Design of a laminated ceramic composite for improved strength and toughness. J Am Ceram Soc 1992; **75**: 3396-400.

13. An L, Chan HM, Padture NP, Lawn BR. Damage-resistant alumina-based layer composites. J Mater Res 1996; **11**: 204-209.

14. Bueno S, Baudín C. Layered materials with high strength and flaw tolerance based on alumina and aluminium titanate. J Eur Ceram Soc 2007; **27**: 1455-1462.

15. De Portu G, Bueno S, Micele L, Baudín C, Pezzotti G. Piezo-spectroscopic characterization of alumina-aluminium titanate laminates. J Eur Ceram Soc 2006; **26**: 2699-2705.

16. Bueno S, Moreno R, Baudín C. Colloidal Processing of Laminates in the System Alumina-Titania. Key Engineering Materials 2004; **264-268**: 61-64.

17. Senda T, Yasuda E, Kaji M, Bradt RC. Effect of grain size on the sliding wear and friction of alumina at elevated temperatures. J Am Ceram Soc 1999; **82**: 1505–1511.

18. Xiong F, Manory RR, Ward L, Terheci M. Effect of grain size and test configuration on the wear behavior of alumina. J Am Ceram Soc 1997; **80**: 1310–1312.

19. Krell A, Klaffke D. Effects of grain size and humidity on fretting wear in fine-grained alumina, Al2O3/TiC, and zirconia. J Am Ceram Soc 1996; **79**: 1139–1146.

20. Guicciardi S, Melandri C, Lucchini F, De Portu G. On data dispersion in pin-on-disk wear tests. Wear 2002*;* **252**: 1001–1006.

21. Tarlazzi A, Roncari E, Pinasco P, Guicciardi S, Melandri C, De Portu G. Tribological Behaviour of Al2O3/ZrO2–ZrO2 Laminated Composites. Wear 2000; **244**: 29–40.

22. Esposito L, Moreno R, Sánchez Herencia AJ, Tucci A. Sliding wear response of an alumina–zirconia system. J Eur Ceram Soc 1998; **18**: 15–22.

23. Luo HH, Zhang FC, Roberts SG. Wear resistance of reaction sintered alumina/mullite composites. Materials Science and Engineering A. 2008; **478**: 270-275.

24. Evans AG. Abrasive Wear in Ceramics: An Assesment. In: Hockey BJ, Rice RW, editors. The Science of Ceramic Machining and Surface Finishing, II, National Bureau of Standards Sp. Pub. 562, US Govt. Printing Office; 1979, p. 1-14.

25. De Portu G, Micele L, Prandstraller D, Palombarini G, Pezzotti G. Abrasive wear in ceramic laminated composites. Wear 2006; **260**: 1104–1111.

26. Bueno S, Moreno R, Baudín C. Reaction sintered Al_2O_3 /Al_2TiO_5 microcrack-free composites obtained by colloidal filtration. J Eur Ceram Soc 2004; **24:** 2785-2791.

27. Sepulveda P, Dos Santos WN, Pandolfelli VC, Bressiani JC, Taylor R. Thermal Conductivity of Gelcast Porous Alumina. American Ceramic Society Bulletin 1999; **78:** 61-66.

28. Kingery WD, Bowen, HK, Uhlmann DR. Thermal Properties. In: Introduction to Ceramics, New York: John Wiley & Sons Inc; 1976, p. 583-644.

29. He YJ, Winnubst AJA, Schipper DJ, Burggraaf AJ, Verweij H. Effects of a second phase on the tribological properties of Al2O3 and ZrO2 ceramics. Wear 1997; **210**: 178–187.

30. Marshall DB, Lawn BR, Evans AG. Elastic/Plastic Indentation Damage in Ceramics: The Lateral Crack System. J Am Ceram Soc 1982; **65**: 561-566.

Figure Captions

Fig. 1. Schematic illustration of the designed laminated structure with five layers showing a bend bar and the notch orientation with respect to the layers.[14] The thick external and central alumina layers (A) are represented with white colour and have a thickness of ≅1800 μm. The thin alumina + 10 vol.% aluminium titanate internal composite layers (AT) are represented with grey colour and have a thickness of ≅300 μm. Dashed lines indicate the position of large grained alumina interfaces due to titania diffusion.

Fig. 2. Photographs showing the pin-specimen support configuration (a) and a detail of the square specimen assembled on the support (b). The specimen rotated above the fixed pin and the load was applied by a lever arm.

Fig. 3. Characteristic microstructures of the studied materials. FE-SEM micrographs of polished and thermally (a, c) or chemically b) etched surfaces. [14]

a) Alumina sintered at 1550ºC.
b) Detail of the laminate showing an alumina-aluminium titanate composite internal layer (intermediate grey) in the centre of the micrograph, two large grained alumina interfaces at both sides (clearest grey) and part of the fine grained alumina layers (dark grey).
c) Detail of the large grained alumina interface (lower half of the image) contiguous to an alumina-aluminium titanate composite internal layer (upper half of the image).

Fig. 4. Characteristic SEM-EDX observations performed on the worn surfaces of WC pins slid against monolithic alumina (a,b) and laminated (c) specimens.

Fig. 5. Characteristic SEM-EDX observations performed on the worn surfaces of the ceramic specimens.

a) Wear track on the reference alumina monolithic specimen
b) Wear track on the surface alumina layer of the laminated specimen
c) Detail of the compacted layer that cover the wear track in the monolithic specimen
d) Detail of the intergranular fracture of the underlying surface in the monolithic specimen
e) Characteristic EDX analysis performed on the intergranular fracture of the worm surface in a monolithic alumina specimen.

Fig. 6. Characteristic SEM-EDX observation of the debris compacted layer along the wear track of an alumina monolithic specimen.

a) SEM observation showing mainly two grey shades randomly distributed.
b) Semiquantitative EDX analysis performed on the dark grey shade (point 1 in 7a).
c) Semiquantitative EDX analysis performed on the lighter shade (point 2 in 7a). Significant higher W contents were found.

Fig. 7. Schematic representation of heat dissipation (Q) from worn surfaces along the monolithic and laminated specimens. Light grey layers represent porous alumina interlayers. K refers to thermal conductivity and h to convection heat transfer coefficient.

Fig. 8. Representation of relative density values (% of theoretical density) for the layers and interfaces in the half of the symmetrical laminated structure. Average values (□) of two determinations (●) are showed. Connecting lines are drawn between the average data points. The dashed line represents the relative density of monolithic alumina materials. Dotted lines

and the photograph (Fig. 3b) are superimposed to clarify the position of layers and interfaces. A: alumina layer, I: interface and AT: alumina+10vol. % aluminium titanate layer.

Figure

Fig. 1

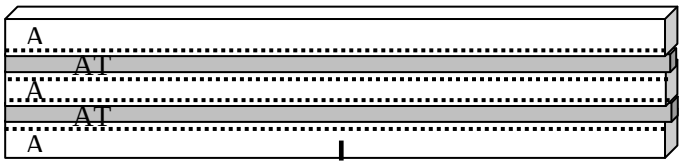

Figure

Fig. 2

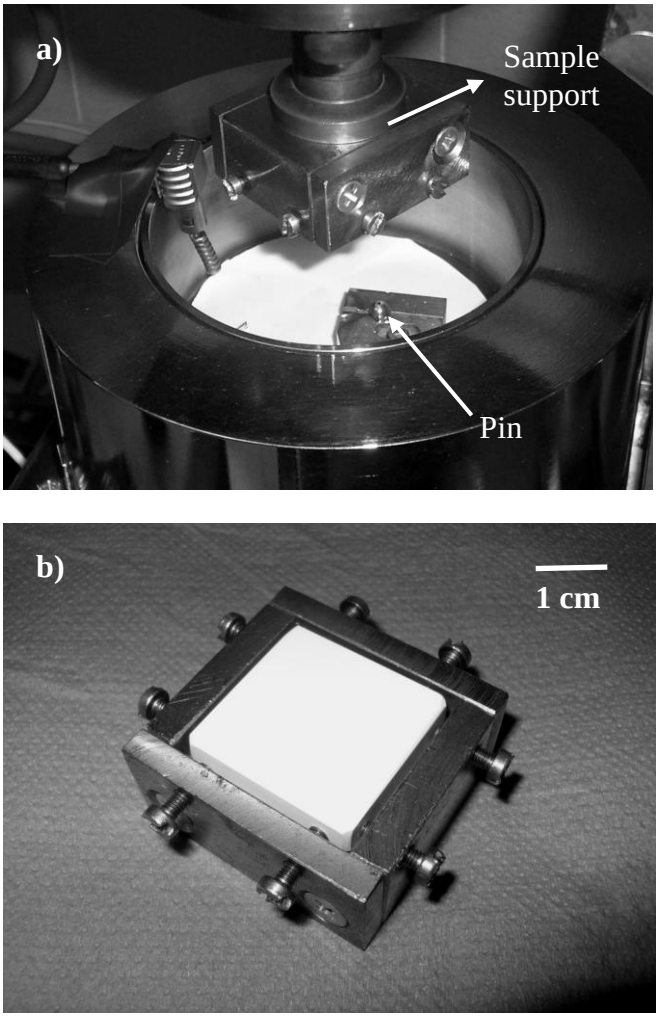

Figure

Fig. 3

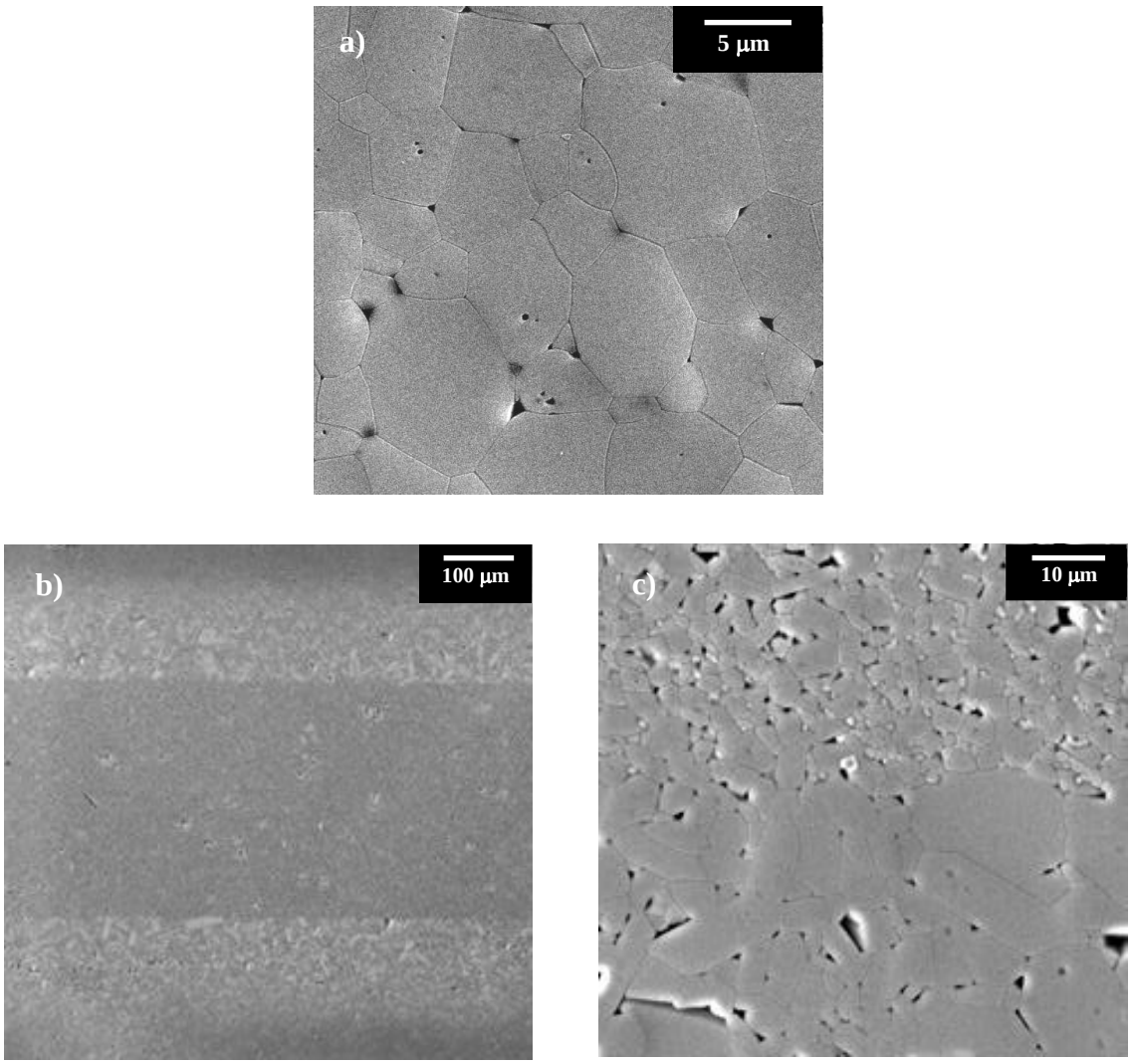

Figure

Fig. 4

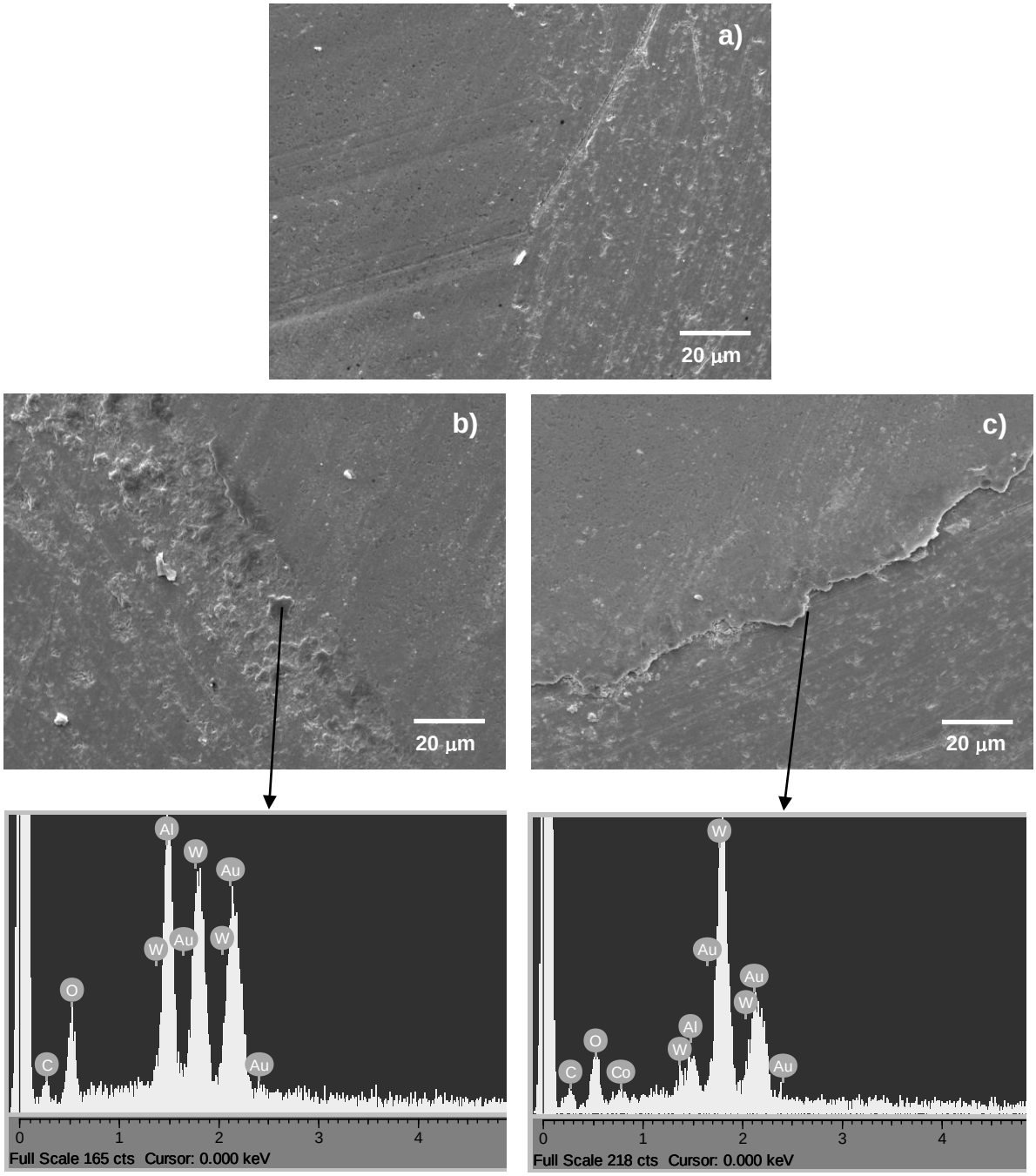
a)
20 μm
b)
20 μm
c)
20 μm
Al
W
Au
W
Au
W
O
C
Au
0
1
2
3
4
Full Scale 165 cts Cursor: 0.000 keV
W
Au
Au
W
Al
O
W
C
Co
Au
0
1
2
3
4
Full Scale 218 cts Cursor: 0.000 keV

Figure

Fig. 5

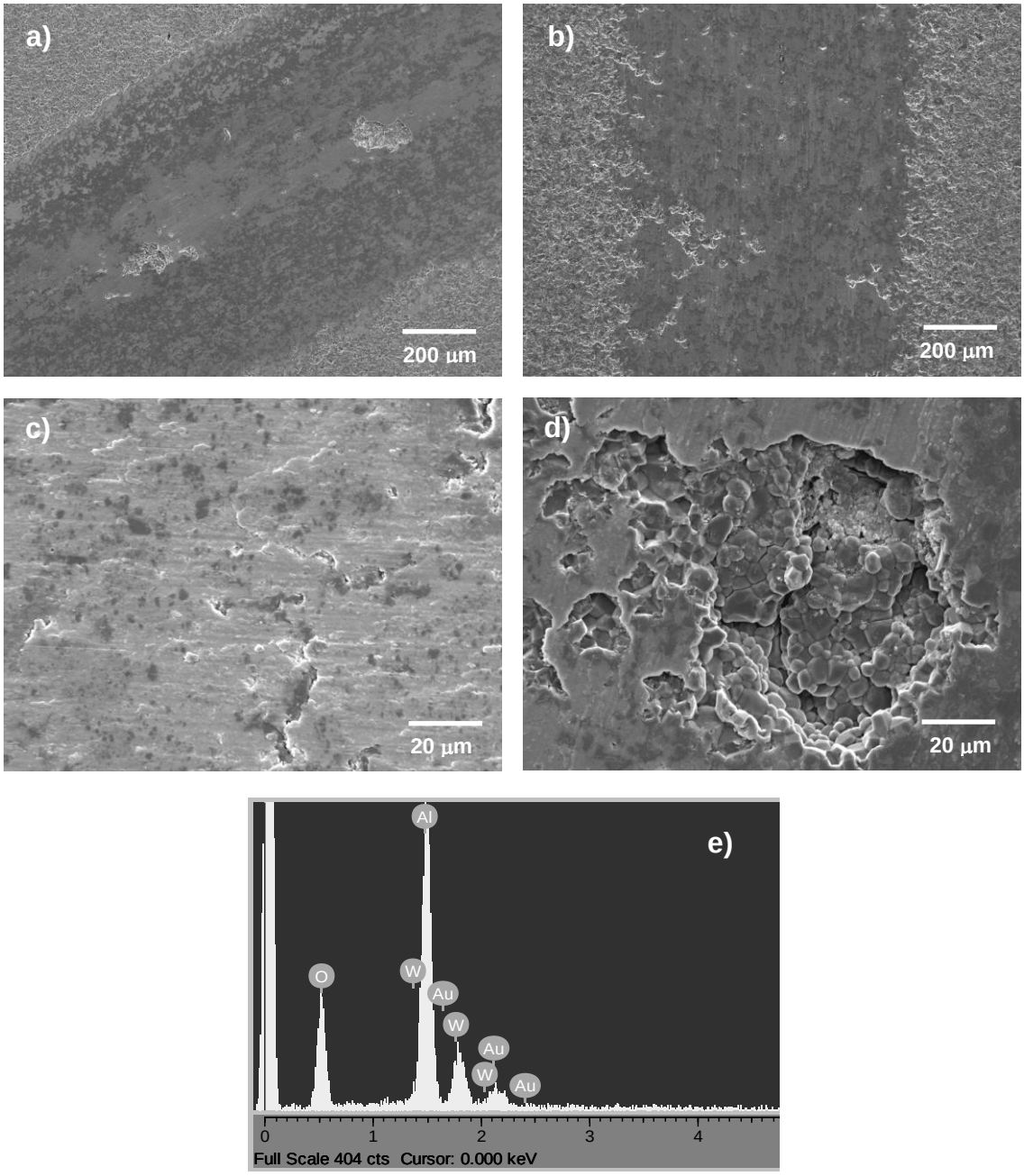
a)
200 μm
b)
200 μm
c)
20 μm
d)
20 μm
e)
Al
O
W
Au
W
Au
W
Au
0
1
2
3
4
Full Scale 404 cts Cursor: 0.000 keV

Figure

Fig. 6

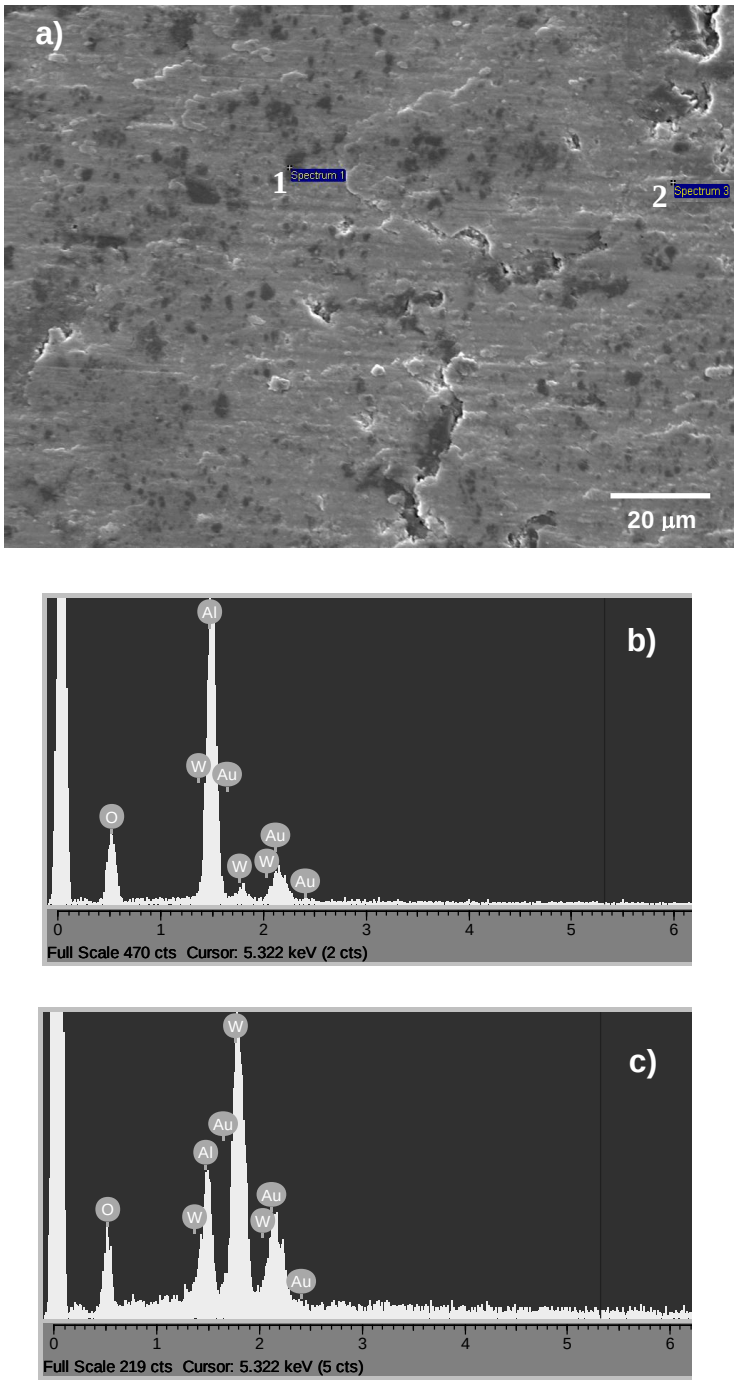
a)
1
Spectrum 1
2
Spectrum 3
20 µm
b)
Al
W
Au
O
Au
W
W
Au
0
1
2
3
4
5
6
Full Scale 470 cts Cursor: 5.322 keV (2 cts)
c)
W
Au
Al
O
W
Au
W
Au
0
1
2
3
4
5
6
Full Scale 219 cts Cursor: 5.322 keV (5 cts)

Figure

Fig. 7

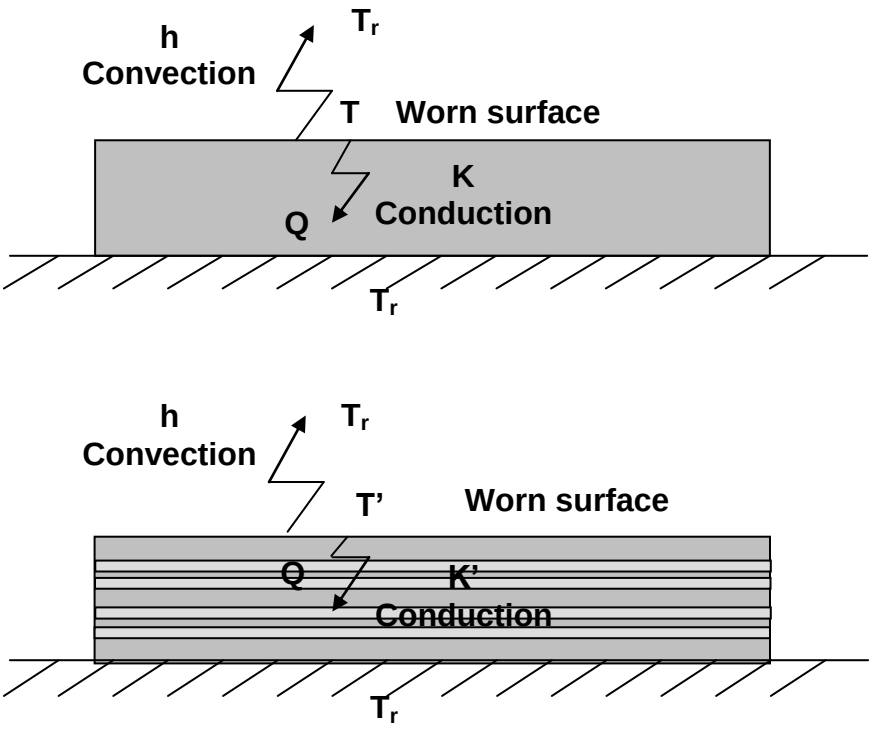
h
Convection
T_r
T
Worn surface
K
Conduction
Q
T_r
h
Convection
T_r
T'
Worn surface
Q
K'
Conduction
T_r

Figure

Fig. 8

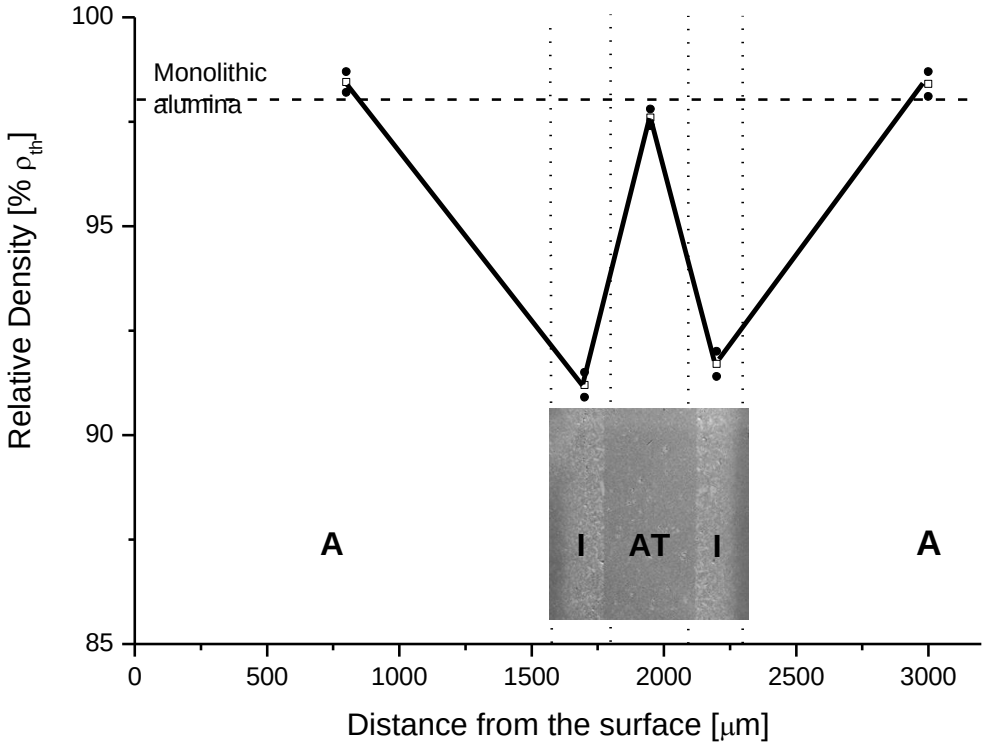
100
95
90
85
Monolithic
alumina
Relative Density [% ρth]
A
I
AT
I
A
0
500
1000
1500
2000
2500
3000
Distance from the surface [μm]

Tables

Table I. Properties of the studied materials. ρ: Density, G_A: Grain size of alumina grains, H_V: Vickers Hardness, σ_f: 3-point bending strength, E: Young's modulus, K_{IC} and γ_{WOF}: Fracture toughness and work of fracture values determined by 3 point SEVNB tests using as relative notch depth a/W=0.15.

		Monolithic alumina	**Laminate**
ρ	(g/cm^3)	3.93 ± 0.01	3.92 ± 0.02
G_A	(μm)	5.5 ± 0.5	5.2 ± 0.3*
H_V	(GPa)	16.8 ± 1.0	17.2 ± 0.3*
σ_f	(MPa)	349 ± 30	-
E	(GPa)	388 ± 5	391 ± 5*
K_{IC}	($MPa \cdot m^{1/2}$)	3.1 ± 0.1	3.5 ± 0.2**
γ_{WOF}	(J/m^2)	20 ± 3	48 ± 1

* Apparent value
** Notches contained within the surface alumina layer

Table II. Average values and standard deviation of wear rates, W, determined on worn pins and ceramic specimens. (A: Reference monolithic alumina; LAM: Laminated structure). *wt* refers to wear evaluated from mass loss and *vol* to wear evaluated from volume loss. f_{tested} is the ratio of W_{vol} and f_{calc} is the ratio of wear resistance calculated with Evans' formula.[23,24]

	PIN		**DISC**			
	W_{wt} ($g/m \cdot N$)	W_{vol} ($mm^3/m \cdot N$)	W_{wt} ($g/m \cdot N$)	W_{vol} ($mm^3/m \cdot N$)	f_{tested}	f_{calc}
A	$(1.1 \pm 0.7) \cdot 10^{-9}$	$(6.5 \pm 2.3) \cdot 10^{-8}$	$(2.3 \pm 2.6) \cdot 10^{-9}$	$(1.2 \pm 0.5) \cdot 10^{-7}$	0.6	0.9
LAM	$(0.4 \pm 0.1) \cdot 10^{-9}$	$(4.2 \pm 0.9) \cdot 10^{-8}$	$(1.1 \pm 2.0) \cdot 10^{-9}$	$(0.7 \pm 0.2) \cdot 10^{-7}$		